IEEE Open Journal of the
Industrial Electronics Society

Received 22 May 2024; accepted 17 June 2024. Date of publication 21 June 2024;
date of current version 3 July 2024. The review of this paper was arranged by Associate Editor Antonio J. Marques Cardoso.

Digital Object Identifier 10.1109/OJIES.2024.3417401

Optimal Robust Time-Domain Feature-Based Bearing Fault and Stator Fault Diagnosis

G. GEETHA AND P. GEETHANJALI

School of Electrical Engineering, Vellore Institute of Technology, Vellore 632014, India

CORRESPONDING AUTHOR: P. GEETHANJALI (e-mail: pgeethanjali@vit.ac.in)

ABSTRACT In machine learning, the extraction of features is necessary for intelligent motor fault diagnosis. In industrial applications, it is necessary to identify the optimal number of features to differentiate various types of fault characteristics with less computational complexity and cost. However, motor fault diagnosis for real-time applications has challenges in capturing characteristics due to variations in speed, load, force, run-to-failure state as well as the type of the motor and its parts. The deep learning techniques that automatically extract features and perform classification have algorithmic complexity. In this work, the authors address these challenges by: 1) selecting and ensembling optimal time-domain features that are capable of identifying motor faults using current signals of the permanent magnet synchronous motor (PMSM) in bearing; and 2) investigating the feature ensemble constituting optimal features for robust fault diagnosis in the PMSM bearing as well as the stator and bearing of squirrel cage induction motor (SCIM) for various conditions. The optimal features mean absolute value, simple sign integral, and waveform length yields 99.8% and 100% for bearing fault and stator fault diagnosis, respectively, in PMSM. These features show 100% accuracy for identification of fault in SCIM and 98.2% accuracy in the run-to-failure state.

INDEX TERMS Induction motor, permanent magnet synchronous motor (PMSM), rolling bearings, stator, deep learning (DL), time-domain features, pattern recognition.

I. INTRODUCTION

Nowadays, permanent magnet synchronous motors (PMSMs) [1] and induction motors [2] have a wide range of applications including electric vehicles as well as industrial automation. In electrical machines, identification of various faults is vital for safe production and avoiding economic losses [3]. According to a recent survey, the majority of mechanical failures are due to bearing defects accounting for 45%–55% [4] and the majority of the electrical faults are due to stator winding exhibiting 21% to 40% [5]. Therefore, researchers instigated to find bearing and stator faults widely using motor current signals.

The fault diagnosis is motivated using deep learning (DL) [6] and pattern recognition [7] approaches to obtain high accuracy. In recent years, DL methods, which flourished globally due to their advanced characteristics, such as automated adaptive feature extraction and greater labeled dataset management. Convolution neural network (CNN) is the most prevalent DL algorithm for the identification of faults. Further researchers transformed the acquired signals into images and found efficacy is excellent. However, these methods have the demerits of a large number of input images leading to the requirement of GPU hardware [8], [9] for a significant amount of memory consumption as well as computations. In real-time industrial settings implementing these techniques is challenging [6]. It is also important to note that DL models may be less effective due to the need for large amounts of data and lengthy training time in industrial processes.

In pattern recognition, the identification of features and classifiers is crucial to recognize intricacies for high accuracy. However, the pattern recognition method [10] does not require GPU for more memory, and computation. In this method, various frequency, time–frequency, and time features are attempted for machine fault diagnosis [11], [12]. The frequency and time–frequency features have better performance in fault diagnosis. However, the extracted features are difficult to manage due to their large size and necessitate feature reduction or selection causing increased computation complexity [13].

Time-domain feature-based extraction methods are simple and fault diagnosis is attempted using conventional features, such as standard deviation, crest factor, peak value, kurtosis (KURT), root-mean-square (rms), shape factor, variance (VAR), and skewness (SKW) [14], [15], with different classifiers such as artificial neural networks, linear discriminant analysis, support vector machine, random forest, decision tree (DT), *k*NN, and naïve Bayes (NB) approaches [10], [16], [17].

The feature selection is usually employed to determine the optimal number of features that greatly improve the speed and maximize the accuracy for fault diagnosis of different electrical machines. Particle swarm optimization (PSO) [18], emperor penguin optimization [19], whale optimization [20], and weighted superposition attraction optimization [21] are the recently employed feature selection methods attempted by researchers.

Our study solely looked at time-domain features that do not require further signal transformation to reduce computation complexity. Therefore, in this study, we investigated the five conventional and five nonconventional time-domain features (NCTDFs) to identify the optimal robust time-domain feature ensemble (FE) for reliable fault diagnosis. The contribution of the work in the identification of the machine faults is as follows in four case studies.

1) The optimal NCTDF and conventional time-domain feature (CTDF) pertinent to individual and combined two different phase current signals are selected using the PSO from the Paderborn University (PU) PMSM bearing database to lessen computation complexity and time. The robustness of the identified four FEs from PSO constituting optimal features is investigated for different speeds, loads, and forces in four different operating conditions.
2) The robustness of the nonconventional optimal FEs is studied with stator fault using PMSM current signal for different fault severity levels.
3) The stability of FEs is also studied at different sampling frequencies with phase current signals at three different load conditions and computationally compared with the AlexNet deep neural network.
4) The adeptness of optimal FEs is studied in the run-to-failure bearing state dataset of the National Aeronautics and Space Administration (NASA).

The rest of this article is organized as follows. In Section II, methodology, which includes the dataset description, windowing, feature extraction, robust feature selection, and pattern recognition-based fault diagnosis. Sections III and IV explore bearing faults and stator fault identification with benchmark datasets. Sections V and VI examine the robustness of the optimal features using experimental squirrel cage induction motor (SCIM) data and run-to-failure bearing dataset. In Section VII, a summary of the results, limitations, and future scope is discussed. Finally, Section VIII concludes this article.

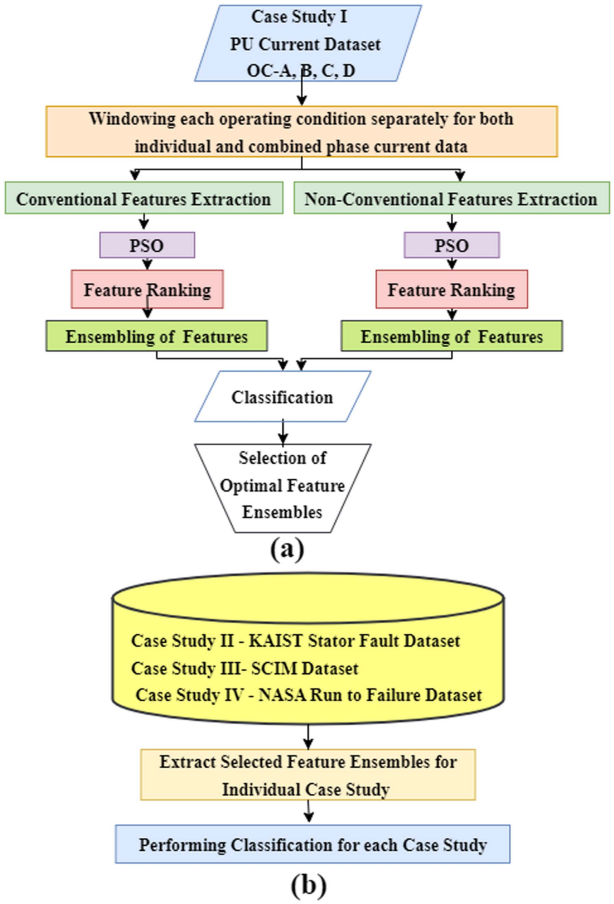

FIGURE 1. Flowchart of the fault diagnosis method. (a) Optimal feature selection. (b) Investigating robustness of the optimal FEs.

TABLE 1. Operating Conditions

Operating conditions (OC)	Speed (RPM)	Load torque (Nm)	Force (N)
A	1500	0.1	1000
B	900	0.7	1000
C	1500	0.7	400
D	1500	0.7	1000

II. FAULT DETECTION METHODOLOGY

The flowchart of the fault diagnosis method is shown in Fig. 1. This study investigates the PMSM in case studies 1 and 2, and the SCIM in case study 3. The run-to-failure bearing dataset is studied in case study 4. In case study 1, four distinct operating conditions current data of a PMSM from the PU bearing database are shown in Table 1. In case study 2, the robustness of FEs is studied with stator fault for different fault severity levels. In case study 3, a laboratory platform was developed to analyze the stability of the identified FE at a lower sampling rate and compared it with the image-driven AlexNet model. In case study 4, the adeptness of FEs is studied in the run-to-failure bearing state dataset. The subsequent sections describe each stage of the fault diagnosis method.

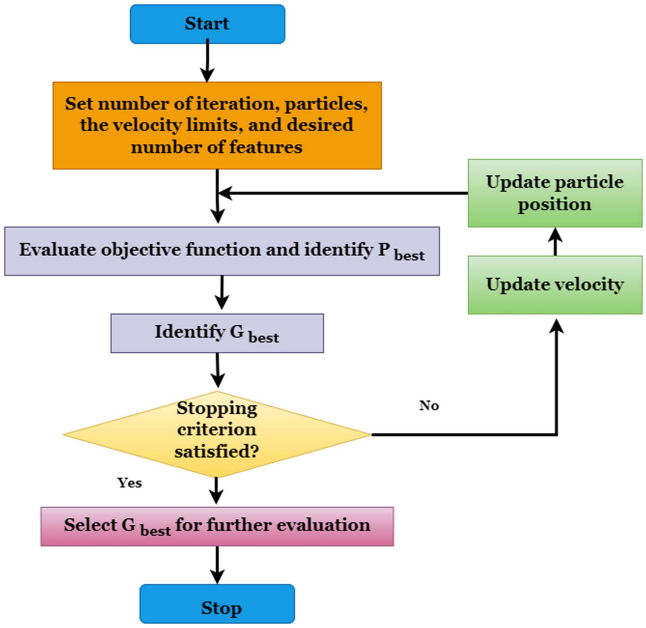

FIGURE 2. Flowchart of feature selection using PSO method.

A. FEATURE EXTRACTION

The most commonly employed CTDFs, including KURT, SKW, mean, rms, and VAR, [22], [23] are evaluated in this article. The NCTDF are mean absolute value (MAV), waveform length (WL), simple sign integral (SSI), slope sign change (SSC), and zero crossing (ZC) extracted [24] to identify optimal robust FEs.

B. OPTIMAL FEATURE SELECTION METHOD

The authors of this article are motivated to find the optimal robust time-domain features to diagnose faults. In case study 1, the PSO algorithm [25] is used to select FEs of size constituting 2, 3, and 4 features for conventional and NCTDFs of current data for four different operating conditions of individual and combined current data. The objective function is to minimize the classification error rate by employing the k nearest neighbor (kNN) classifier. Each particle stands for a solution in the $''M''$ dimensional search space of 5. The particles within the search space undergo movement to locate the most optimal solution for the given objective function.

Fig. 2 depicts the flowchart illustrating the PSO algorithm. Let $i = \{y1, y2, y3, \ldots, yn\}$ represent a set of particles that are initialized with random positions in an M-dimensional search space. Let $y_j^{(t)}$ represent the current position and $v_j^{(t)}$ represent the current velocity for the jth particle at the tth iteration. The objective function is computed for every particle during the tth iteration. The variable $P_{\text{best}(j)}$ represents the personal best position of the jth particle, while G_{best} refers to the best position among all particles in the entire population. The velocity and position of the particles updated at the end of the iteration are shown in (1) and (2). The objective function is evaluated for the newly obtained location, to update $P_{\text{best}(j)}$ and G_{best}. Repeat the steps, when the required number of iterations is reached. Choose the optimal feature subset that G_{best} represents. Utilizing the features that were selected on the test data, evaluate the classifier's performance. This work ranks conventional and NCTDFs separately using PSO

$$v_j^{t+1} = \theta_j^t + \alpha\varepsilon_1\left(P_{\text{best}(j)} - y_j^t\right) + \beta\varepsilon_2\left(G_{\text{best}(j)} - y_j^t\right) \quad (1)$$

$$y_j^{t+1} = y_j^t + v_j^{t+1} \quad (2)$$

where θ is the inertia constant, ε_1, ε_2 are random variables between 0 and 1, and α and β are learning parameters.

C. FEATURE ENSEMBLING

The PSO ranking is used for organizing FEs. The first two rank features are ensembled into FE-2 similarly, FE-3 constitutes the first three ranked features, FE-4 constitutes the first four ranked features, and FE-5 constitutes all five features. The ranked features are ensembled separately for both conventional and nonconventional features for individual and combined current signals.

D. CLASSIFICATION

1) PATTERN RECOGNITION-BASED CLASSIFICATION

In this work, identified FEs are classified for 10% holdout validation using the kNN, DT, and NB classifiers to find the computationally simple classifier. The kNN is one of the simplest pattern recognition algorithms. The kNN method [10] has two fundamental components: distance measurement and k-value selection. Among these, the choice of k value will influence the kNN output. In this work, $k = 3$ is considered for fault diagnosis. The utilization of distance measures facilitates the formation of decision borders, which effectively separates data points into distinct classes. Euclidean distance metrics are employed to determine the closeness of data points.

The DT method is one of the pattern recognition methods [17] is created by choosing a feature with the highest ability as a node to discriminate fault the Gini index used to split the tree's nodes until the model reaches its maximum depth. The NB classifier is a Bayesian classifier that builds its probabilistic model using the maximum likelihood conditions and Bayes' theorem [17]. If the features are well stated, the Bayes classifier achieves the lowest percentage of errors.

2) DL METHOD

In this work, authors attempted a DL AlexNet model [26], constituting five convolutional layers and three fully connected layers. Maxpooling layers are employed after convolutional layers 1, 2, and 5 effectively decrease spatial dimensions while preserving prominent features. AlexNet-based fault diagnosis methods include data acquisition, image conversion, image augmentation, and fault classification. In this work, the acquired SCIM current signals are converted into spectrogram images. In practice, gathering the required information to train a deep neural network for fault classification adequately is challenging. Therefore, the acquired data are converted into an image followed by augmentation

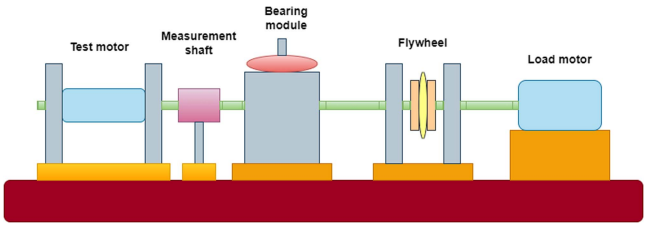

FIGURE 3. Structural sketch of PU dataset.

TABLE 2. Bearing Codes Used (Model No-6203)

Class	Bearing conditions	Bearing codes used
H	Healthy	K001, K002, K003, K004, K005
ORF	Outer race fault	KA04, KA15, KA16, KA22, KA30
IRF	Inner race fault	KI04, KI14, KI16, KI18, KI21

to enhance training samples and to prevent model overfitting. Images may be augmented by mirroring, rotating, vertical flip, horizontal flip, transpose, and elastic transform, the original image dataset is enlarged to several times its original size and finally classified into fully connected layers.

III. CASE STUDY 1: FEATURE SELECTION AND ENSEMBLING OF FEATURES

This case study focuses on the identification of an optimal features ensemble from conventional and nonconventional features using PSO for individual current, and combined two different phase current signals. The ranked conventional and nonconventional features are ensembled of sizes 2, 3, 4, 5, and classified for four different operating conditions.

A. DATASET DESCRIPTION

The structural sketch of the PMSM experiment setup shown in Fig. 3 consists of a test motor, measurement shaft, bearing module (deep groove ball bearing type-6203), flywheel, and load motor. The current in each phase of the test motor rated 425 W, 3000 rpm, 2.3 amps is sampled at 64 kHz for 40 s for four operating conditions of healthy (H), outer race fault (ORF), and inner race fault (IRF) bearings. Table 2 shows the bearing codes used in this work.

B. FEATURE EXTRACTION

Each feature is extracted from a data segment of 64 000 samples for 20 trials of current data. Each trial constitutes 20 data segments accounting for $20 \times 20 = 400$ number of individual features for each fault condition. The combined two-phase current data accounts for 800 individual features for each bearing condition.

C. OPTIMAL FEATURE SELECTION

The PSO algorithm ranks features of all operating conditions separately from the individual and combined current data. The PSO population size is initialized to 50 and the number of iterations is set to 100. The hyperparameters of the PSO algorithm are tuned iteratively and chosen as follows: inertia weight w is 0.2562, the damping ratio of the inertia weight is 0.99, the cognitive coefficient is 1, the social coefficient is 2, and the velocity limit is 0.1, and the variable boundary is 0 to 1. Initially, the ranking sequence of conventional and nonconventional features are {SKW, MEAN, RMS, VAR, KURT} and {SSC, SSI, WL, MAV, ZC}, respectively. At the end of the iterations, the ranking sequence of conventional features is {KURT, SKW, MEAN, RMS, VAR} and nonconventional features {MAV, SSI, WL, SSC, ZC}. The ranked features are ensembled separately for both conventional and nonconventional features, as shown in Table 3.

TABLE 3. FEs Based on the PSO Ranking

FEs	Conventional FEs	Nonconventional FEs
FE-2	{KURT, SKW}	{MAV, WL}
FE-3	{Mean, KURT, SKW}	{MAV, SSI, WL}
FE-4	{Mean, rms, KURT, SKW}	{MAV, WL, SSI, SSC}
FE-5	{Mean, rms, VAR KURT, SKW}	{MAV, SSI, WL, SSC, ZC}

D. CLASSIFICATION

In this section, bearing fault classification using kNN, DT, and NB classifiers with 10% holdout validation is studied. The performance of the identified FE is classified with individual and combined different phase current signals for conventional and nonconventional features for all operating conditions.

1) PERFORMANCE OF CONVENTIONAL AND NONCONVENTIONAL FES

The classification performance of conventional and NCTDFs for operating condition-A of individual and combined two different phase current signals are shown in Fig. 4. For individual phase current signal, it is noted from Fig. 4(a) conventional features, that the classification accuracy shows the highest accuracy of 85% with FEs consisting {KURT, SKW, mean} using kNN classifier. The nonconventional features ensembles consisting of FE-3 {MAV, SSI, WL} yield a maximum of 96% accuracy with kNN classifier higher than DT and NB classifiers. Therefore, it is clear from Fig. 4(a) that nonconventional features perform better than CTDFs.

For combined phase current signals 1 and 2, it is noted from Fig. 4(b) the conventional FE-3 {KURT, SKW, mean} attained the highest accuracy of 94.3% with the kNN classifier. The performance of the nonconventional FE with kNN classifier yields the highest accuracy of 100% with FE-3 {MAV, SSI, WL} and FE-4 {MAV, SSI, WL, SSC}, 2.9% higher than the DT classifier. The FE-2 yields 1.7% less than FE-3 and FE-4 using the kNN classifier. The performance of the NB classifier is less with conventional and nonconventional FEs

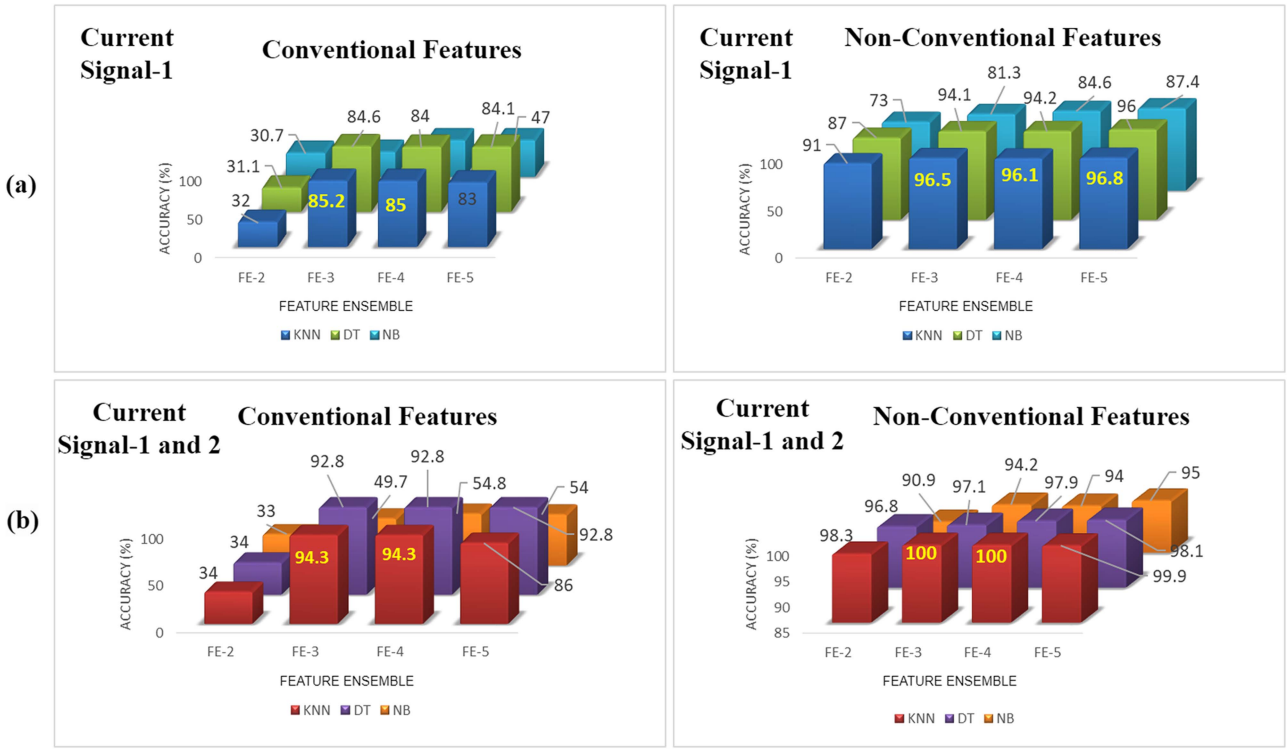

FIGURE 4. Classification performance of optimal conventional FEs and nonconventional optimal FEs. (a) Individual phase current signal. (b) Combined phase current signals.

in comparison with *k*NN and DT classifiers considered. From Fig. 4(b), it is clear that the CTDF ensembles do not perform well in comparison with the NCTDF ensembles. Also, FE-3 performance is significantly not different from FE-4 and FE-5.

The classification performance reveals that the NCTDF ensembles with combined two-phase current signals perform better and show higher fault classification accuracy. Therefore, the nonconventional FEs FE-2{MAV, SSI}, FE-3 {MAV, SSI, WL}, FE-4 {MAV, SSI, WL, SSC}, and FE-5 {MAV, SSI, WL, SSC, ZC} have been considered for further studies.

2) IMPACT OF SELECTED FES FOR DIFFERENT OPERATING CONDITIONS

Further studies investigate the efficacy of the identified FEs using the combined phase current signals under three different operating conditions in addition to operating condition A. The classification performance of the varying combination of combined two-phase current signals is depicted in Fig. 5 for four distinct operating conditions. From Fig. 5, it is clear that the FE-3 shows 100% with the *k*NN classifier for operating conditions A, B, and D. In operating condition C, the identified FE-3 has shown 99.2% accuracy. The FE-2 yields an average classification accuracy of 98.5% with *k*NN. The average classification accuracy of FE-3 shows 97.3% and 94% accuracy with the DT and NB classifiers, respectively, under four operating conditions. It shows a statistically significant difference in the performance of the NB classifier compared with a DT and *k*NN classifiers. In addition, the *k*NN classifier is shown to be statistically insignificant with FEs FE-3, FE-4, and FE-5.

It is clear from Fig. 5, that FE-3 {MAV, SSI, WL} was found to be optimal in comparison with identified FEs with high accuracy for combined current signals under four operating conditions using *k*NN classifier.

In addition to classification accuracy other performance metrics including sensitivity, specificity, precision, F1 score, false positive rate (FPR), and false negative rate (FNR) are also calculated as shown in Table 4 for comparison of classifiers considered. These metrics were calculated for combined current signals. It is clear from Table 4, that the optimal FE {MAV, SSI, WL} achieved the highest performance using the *k*NN classifier in comparison with DT and NB classifiers under four different operating conditions.

Feature plots are employed to analyze the discriminating ability of each identified optimal NCTDF. Data have been collected for three distinct bearing conditions, as depicted in Fig. 6. The variation of the feature value to the window segment for healthy, inner, and ORFs is shown. Accordingly, the variation of each utilized feature of three different bearing conditions is plotted. It is clear from Fig. 6, that optimal nonconventional features mean absolute value, SSI, and WL was an effective feature that maintained the most separability between three bearing classes among all studied four operating conditions A, B, C, and D. In addition, the SSC and ZC shows least variation in comparison with identified optimal features.

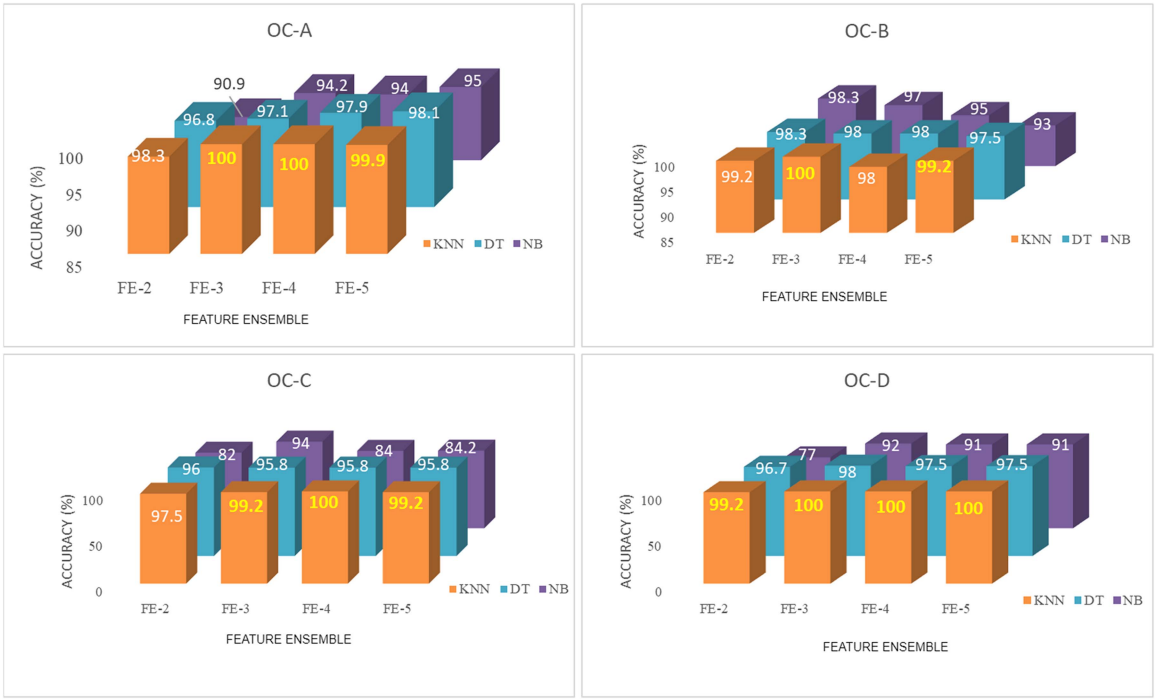

FIGURE 5. PMSM bearing fault classification accuracy using combined current signal under four operating conditions.

TABLE 4. Performance Index of Combined Current Signals

Performance index combined current	OC-A			OC-B			OC-C			OC-D		
	kNN	DT	NB	kNN	DT	NB	kNN	DT	NB	kNN	DT	NB
Sensitivity	1	0.9674	0.9771	1	0.9768	0.9876	0.9987	0.9876	0.9766	1	0.9969	0.9608
Specificity	1	0.8923	0.7684	1	0.8622	0.9387	0.9935	0.6052	0.8682	1	0.7982	0.8331
Precision	1	0.9756	0.9412	1	0.9679	0.9867	0.9987	0.8809	0.9401	1	0.9502	0.9608
F1 score	1	0.9715	0.9588	1	0.9723	0.9871	0.9987	0.9312	0.9580	1	0.9730	0.9604
FPR	0	0.1077	0.2316	0	0.1378	0.0613	0.0065	0.3948	0.1318	0	0.2018	0.667
FNR	0	0.0326	0.0229	0	0.0232	0.0124	0.0013	0.0124	0.0234	0	0.0031	0.0392

IV. CASE STUDY 2:INVESTIGATING THE ROBUSTNESS OF FES FOR STATOR FAULT IDENTIFICATION

This case study investigates the robustness of the identified FEs in PMSM stator interturn fault identification using current signals under eight fault severity levels from the Korea Advanced Institute of Science and Technology (KAIST) dataset [27].

A. DATASET DESCRIPTION

The experimental setup comprises a 1 kW PMSM and a load controller with a hysteresis brake. The parameter specification of the PMSM is shown in Table 5. The three-phase current data were obtained with the Hioki CT6700 model. The data were recorded using a National Instrument 9775 module with a 100 kHz sampling frequency for 120 s. Table 6 shows the PMSM stator interturn fault severities with class labels.

B. FEATURE EXTRACTION

Each feature is extracted from a data segment of 100 000 samples. It constitutes 120 data segments accounting for 120 individual features for each fault severity level.

TABLE 5. PMSM Parameters for Stator Fault Diagnosis

Parameters	Specifications
Rated power	1000 W
Rated speed	3000 RPM
Rated torque	3.18 Nm
Number of phase	3
Number of pole	4
Input voltage	380 V

TABLE 6. Class Label for Stator Interturn Fault in PMSM

Fault label	Fault severity (%)
1	0
2	2.26
3	2.70
4	3.35
5	4.41
6	6.48
7	12.17
8	21.69

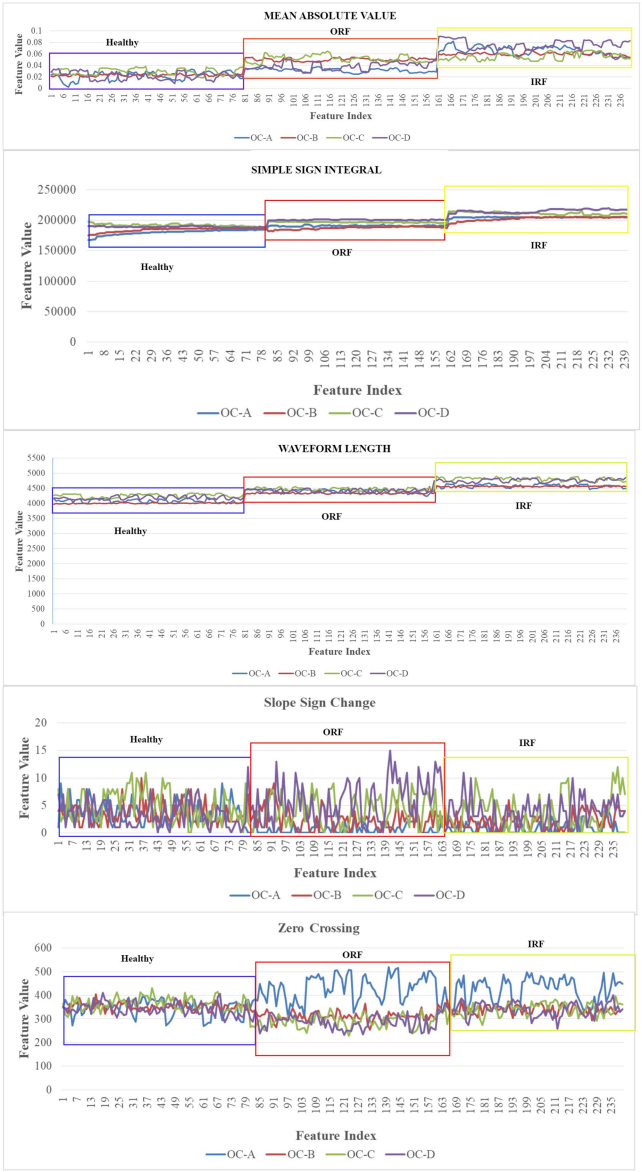

FIGURE 6. Feature plot of three bearing conditions.

C. CLASSIFICATION

The classification performance studied with the identified nonconventional FEs using current signals. The identified FEs FE-2, FE-3, FE-4, and FE-5 classification accuracy are shown for three-phase current signals. From Fig. 7, it can be observed that the classification accuracy for the phase current signal is 98%–100%. The high accuracy is achieved specifically FE-3, FE-4, and FE-5, with the *k*NN classifier. The FE-3 {MAV, SSI, WL} yields an average accuracy of 99.3% with current data using the *k*NN classifier.

The *k*NN and DT classifiers are statistically insignificant with the FE-3, FE-4, and FE-5 compared to the NB classifier. It shows a statistically significant difference in the performance of the FE-2 with FE-3, FE-4, and FE-5 for individual phase current signals. The average accuracy of 100% is achieved using a combined current signal FE-2, FE-3, FE-4, and FE-5 with *k*NN, and DT classifiers. The *k*NN, DT, and NB classifiers show no statistically significant difference with the combined phase current signals. It is clear from Fig. 7, that as the number of fault severity increases individual phase current data is sufficient to identify the fault in PMSM for stator fault identification. The performance metrics were calculated for three-phase PMSM current signals. It is clear from Table 7, that the optimal FE-3 {MAV, SSI, WL} achieved the highest performance using the *k*NN classifier in comparison with DT and NB classifiers.

V. CASE STUDY 3: INVESTIGATING THE STABILITY OF FES IN SCIM

The identified FEs achieved good diagnostic performance for PMSM bearing and stator interturn fault diagnosis. Consequently, this case study examines the stability of the identified FEs in a SCIM bearing faults using three-phase SCIM current signals at different sampling rates.

A. EXPERIMENTAL SETUP DESCRIPTION

The test platform includes a 3.73 kW, 7 A, and 1500 RPM SCIM coupled to a 5 HP dc generator powering a resistive load. The ball-bearing parameters are shown in Table 8. The Compact-RIO is used to acquire the three-phase SCIM current signal through the three-channel current input module NI-9246 using LabVIEW software. The NI 9246 current input module employs a combination approach, utilizing analog and digital filtering techniques. The key bandwidths to be considered are the passband, the stopband, and the anti-imaging bandwidth. The experimental setup sketch is depicted in Fig. 8.

Three-phase current signals are acquired for healthy, ORF, and ball faults for 40 s over two trials at sampling frequencies of 3125 Hz and 16 and 50 kHz under no load, half load, and full load conditions. Two different bearing faults are considered in this experiment including the ORF and the ball fault. The electrical discharge machining used to create the outer race artificial bearing damage of 2.5 mm in depth and 6 mm in diameter [28], and lifetime ball damage is considered.

B. FEATURE EXTRACTION

The NCTDFs are extracted from 3125, 16 000, and 50 000 samples for two trials of three-phase current data constituting 40 data segments accounting for $2 \times 40 = 80$ feature individual.

C. CLASSIFICATION

The stability of the identified NCTDF ensembles has been studied experimentally using motor current signals. The bearing conditions at three different lower sampling frequencies are tested for three combinations of current signals {R $\wedge$ Y, Y $\wedge$ B, B $\wedge$ R} at different load conditions.

The classification performance under 3125 Hz is shown in Fig. 9. It can be observed that at no load conditions, classification accuracy was greater than 94.6% with identified FEs using the *k*NN classifier. The DT and NB classifiers showed

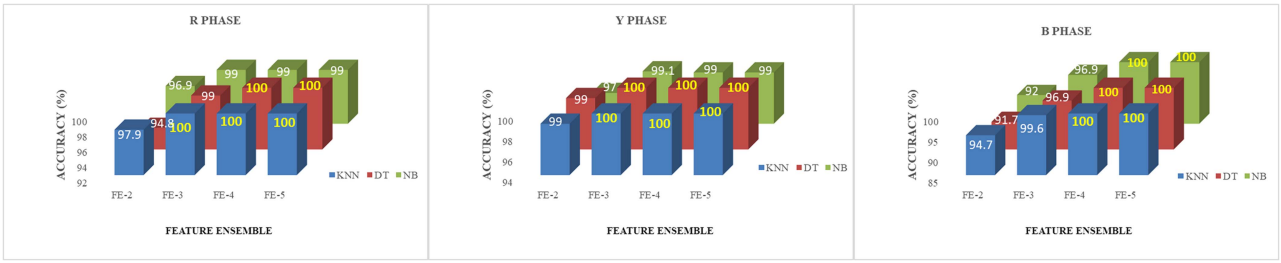

FIGURE 7. Classification accuracy of stator interturn fault using motor current signals.

TABLE 7. Performance Index of Stator Fault Diagnosis Using Current Signal

Performance index	R phase			Y phase			B phase		
	kNN	DT	NB	kNN	DT	NB	kNN	DT	NB
Sensitivity	1	0.9987	0.9958	1	1	0.9968	0.9978	0.9873	0.9565
Specificity	1	0.9744	0.9943	1	1	0.9912	0.9632	0.7918	0.8619
Precision	1	0.9915	0.9981	1	1	0.9971	0.9915	0.9201	0.9497
F1 score	1	0.9951	0.9970	1	1	0.9970	0.9946	0.9525	0.9426
FPR	0	0.0256	0.0057	0	0	0.0088	0.0368	0.2082	0.1381
FNR	0	0.0013	0.0042	0	0	0.0032	0.0022	0.0799	0.0035

TABLE 8. SCIM Bearing Specifications

Bearing parameters	Specification/dimension
Bearing model	6306 (deep groove ball bearing)
Number of balls	7
Inner diameter	30 mm
Outer diameter	72 mm
Ball diameter	19 mm

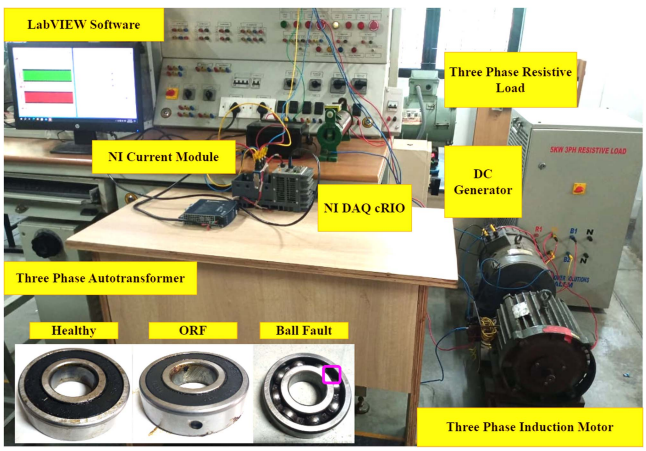

FIGURE 8. Experimental setup.

greater than 92% and 91% accuracy respectively for the R $\wedge$ Y combination. In B $\wedge$ R combination, the *k*NN classifier attained greater than 93% accuracy with FE-2, FE-3, FE-4, and FE-5. The *k*NN classifier is statistically insignificant with all the FEs compared to DT and NB classifiers.

The classification performance under 16 kHz is shown in Fig. 10. At no load conditions, the optimal FE FE-3 {MAV, SSI, WL} observed with 100% accuracy with *k*NN and DT classifiers for R $\wedge$ Y, Y $\wedge$ B, and B $\wedge$ R combinations. The NB classifier obtained a maximum of 77% accuracy with FE-3. The FE-3, FE-4, and FE-5 are statistically insignificant with *k*NN and DT classifiers compared to FE-2. At half and full load conditions FE-3, FE-4, and FE-5 obtained 100% accuracy with *k*NN and DT classifiers under 3125 Hz, and 16 and 50 kHz. The FE-5 attained a maximum of 84% accuracy with the NB classifier. It shows a statistically significant difference in the classification performance of the NB classifier compared with *k*NN and DT classifiers.

The performance metrics were calculated for SCIM current signals under no load, half load, and full load conditions. It is clear from Table 9, that the optimal features {MAV, SSI, WL} achieved the highest performance using the *k*NN classifier in comparison with other classifiers. It is clear from Table 10, as the sampling frequency increases and shows better accuracy using *k*NN and DT classifiers. In 50 kHz sampling frequency, the FEs FE-2, FE-3, FE-4, and FE-5 have shown higher accuracy. However, the identified feature-based fault diagnosis methodology has shown better accuracy even with lower sampling frequency.

The bearing fault classification accuracy of FE-3 has shown a maximum accuracy of 95% with fewer samples (3125 HZ) and 100% with a large number of samples (16 and 50 kHz). Therefore, the optimal robust FE-3 {MAV, SSI, WL} performs well with lower sampling frequencies using SCIM phase current signals.

D. CLASSIFICATION USING ALEXNET

The SCIM current signals were investigated and evaluated using the AlexNet method. The AlexNet model was implemented on 8 GB of memory, an Intel i5 core, a 2.90 GHz processor, and 64-bit operating systems. AlexNet model is trained with 4000 images and tested with 1000 images for each bearing condition. The batch size is 64, and the epoch is 30. Table 11 shows the bearing fault classification accuracy for three different phase current combinations. It can be seen

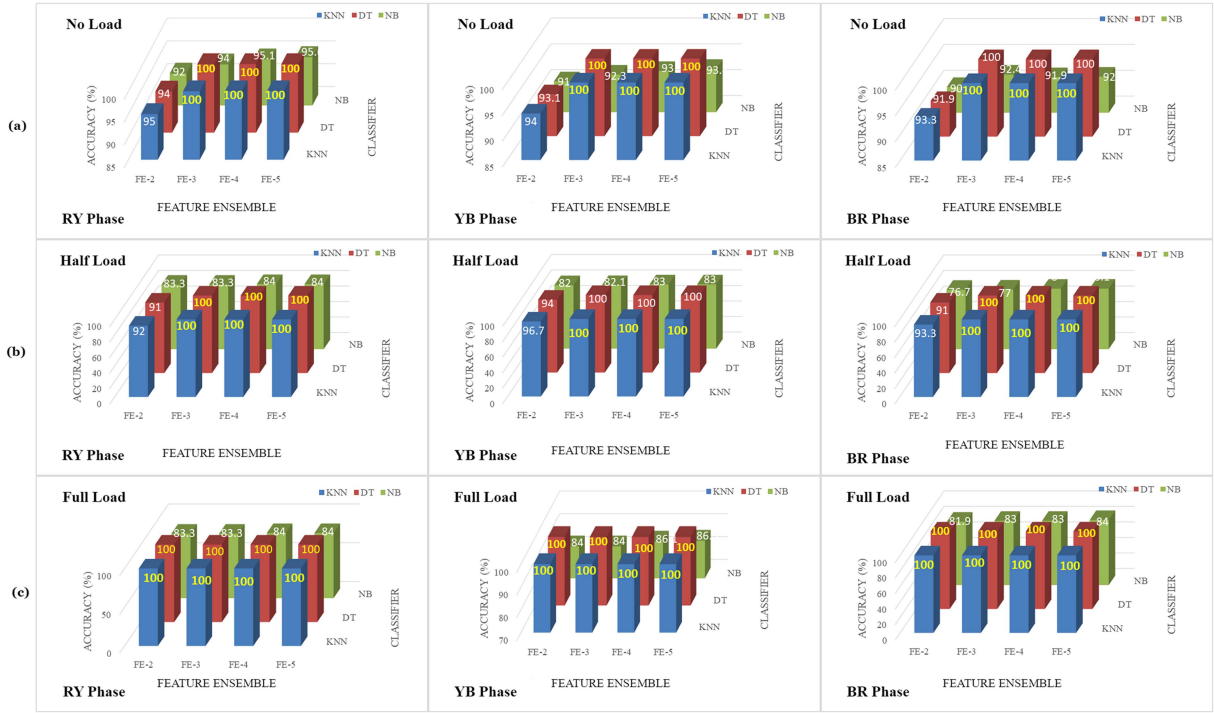

FIGURE 9. Pattern recognition method-based classification accuracy under 3125 Hz sampling frequency.

TABLE 9. Performance Index of Bearing Fault Diagnosis Using SCIM Current Signal

Performance index	No load			Half load			Full load		
	kNN	DT	NB	kNN	DT	NB	kNN	DT	NB
Sensitivity	1	1	0.8750	1	1	0.8818	1	1	0.9868
Specificity	1	1	0.3333	1	1	0.4213	1	1	0.5859
Precision	1	1	0.9608	1	1	0.9593	1	1	0.9786
F1 score	1	1	0.9159	1	1	0.9189	1	1	0.9827
FPR	0	0	0.6667	0	0	0.5787	0	0	0.4141
FNR	0	0	0.0392	0	0	0.1182	0	0	0.0132

TABLE 10. Classification Performance Under Different Sampling Frequencies

FEs	3125 Hz			16 kHz			50 kHz		
	*k*NN	DT	NB	*k*NN	DT	NB	*k*NN	DT	NB
FE-2	94	93	91	95	94	92	100	99.2	94
FE-3	95.6	93	93	100	100	94	100	100	96.7
FE-4	95.6	93.3	92	100	100	95.1	100	100	99.2
FE-5	95.8	95	91.2	100	100	95.6	100	100	99.8

TABLE 11. Fault Classification Accuracy Using AlexNet Method

Phase combination	Accuracy (%)
R phase Y phase	99.40
Y phase B phase	98.01
B phase R phase	98.73
Average	**98.7**

that the AlexNet method-based image classification for three combinations {R ∧ Y}, {Y ∧ B}, and {B ∧ R} phase current data has shown an average accuracy of 98.7% with computation time of 134 min, which is 71% higher than the optimal FE-based fault diagnosis method.

VI. CASE STUDY 4: INVESTIGATING THE ADEPTNESS OF OPTIMAL FES IN RUN-TO-FAILURE STATE

This case study examines the adeptness of the optimal FEs in bearing faults using a run-to-failure NASA bearing dataset. A shaft has four bearings installed on it. Throughout the bearing's expected life of over one hundred million revolutions, faults in the bearing started to appear.

A. EXPERIMENTAL SETUP

Intelligent maintenance systems (IMS) at the University of Cincinnati conducts experiments consisting of run-to-failure bearings datasets [29]. The experimental sketch is depicted in Fig. 11. Four bearings were mounted onto a shaft under

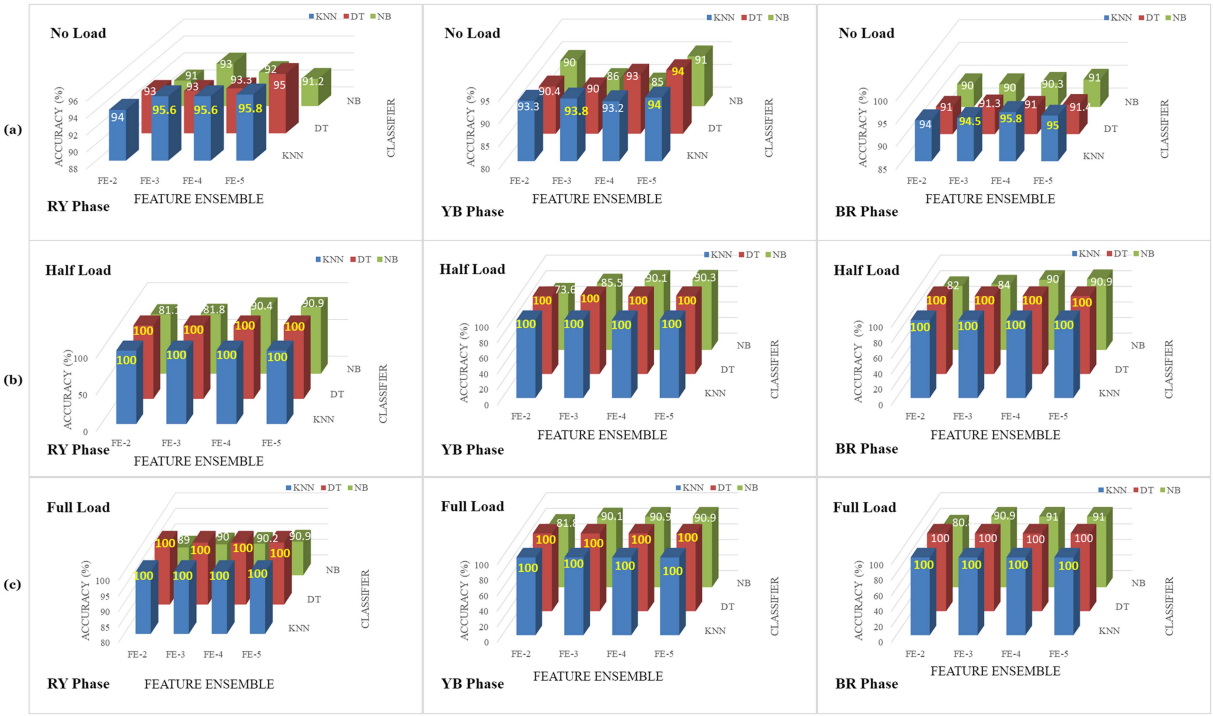

FIGURE 10. Pattern recognition method-based classification accuracy under 16 kHz sampling frequency.

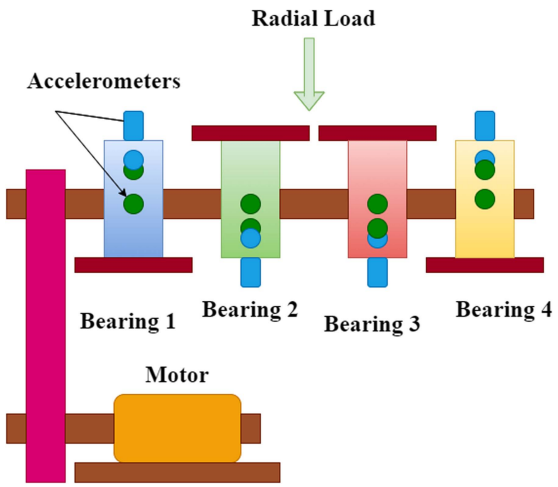

FIGURE 11. Experimental sketch.

the effect of a radial load. The rotational velocity of the shaft remains constant at 2000 revolutions per minute. The shaft is subjected to a radial stress of 6000 lbs. Signals were captured on each bearing, with a sampling frequency of 20 kHz for 1 s, and data were recorded every 10 min.

B. DATASET DESCRIPTION

In this work, recordings of four healthy bearings started on 12th February with 81 recordings and recording stopped on 19th February with 39 recordings was considered for 10% holdout validation. Transient data recorded on 17th February with 144 recordings are used for testing the robustness of the proposed feature-based approach. Run-to-failure occurred only in bearing 1 on 19th February. Table 12 shows the class label with bearing conditions considered.

TABLE 12. Class Label Considered

Class	Condition	Bearing no.	Date
1	Healthy	B1	Feb-12
2	Fault	B1	Feb-19
3	Healthy	B2	Feb-12 and 19
4	Healthy	B3	Feb-12 and 19
5	Healthy	B4	Feb-12 and 19

C. FEATURE EXTRACTION

Each identified NCTDF is extracted from a data segment of 20 000 samples, 81 recordings for healthy data, 39 recordings for fault data considered, and 144 recordings for transient data for testing the proposed method. The data constitutes one data segment for each recording.

D. CLASSIFICATION

In this work, the adeptness of identified FEs is classified for 10% holdout validation using the *k*NN, DT, and NB classifiers for five class classifications.

The identified FEs FE-2, FE-3, FE-4, and FE-5 classification accuracy are shown in Fig. 12. It is clear from Fig. 12, that the optimal FE of FE-3 {MAV, SSI, WL} has shown higher accuracy of 100% using *k*NN and DT classifiers. The FE-2 has shown an accuracy of 97.9% with *k*NN and 96.4% with the DT classifier. The FEs, FE-3 {MAV, SSI, WL}, FE-4

TABLE 13. Time–Frequency Features and Machine Learning Based Related Reference Works

Reference work	Methodology	Current	CS-1∧CS-2
Lessmeier et al. [30]	Wavelet packet decomposition	–	93.3
Nishat et al. [31]	Discrete wavelet transform	99	–
Proposed method	Time-domain features	99	99.8

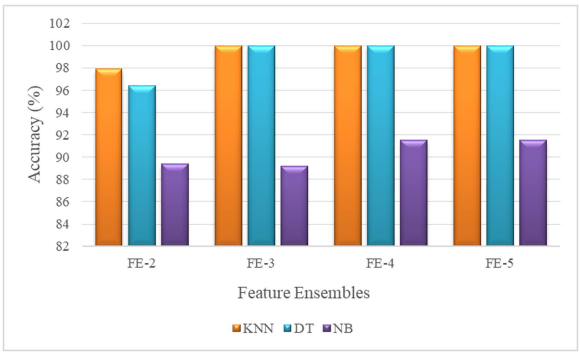

FIGURE 12. Classification performance of run-to-failure bearing fault diagnosis.

{MAV, SSI, WL, SSC}, and FE-5 {MAV, SSI, WL, SSC, ZC} are performing better with an average accuracy of 100% using kNN classifier and NB classifiers shown least performance of 91% accuracy.

VII. DISCUSSION

It is necessary to identify optimal robust features from motor signals concerning different operating conditions, faults in motor parts, faults in different motors, and variations from run-to-failure motor states. In this work, the authors address two goals: 1) selecting and ensembling optimal features that are capable of identifying motor faults using current signals in PMSM and; 2) investigating the FE constituting optimal features for robust fault diagnosis in the PMSM bearing as well as the stator and bearing of SCIM for various conditions.

In case study I, the selection of the robust FE using PSO from the motor current signal was evaluated using the classification performance of each FE. It is noted, that the optimal conventional FE shows the highest accuracy. The optimal FE of three combinations of FE-3 has better performance using individual, and combined phase current signals. This implies that choosing a robust time-domain FE can increase classification accuracy. The impact of robust NCTDFs under different operating conditions is investigated in our study.

In this section, the classification performance of robust FE-based pattern recognition results are compared with the results of similar fault datasets attempted in the literature. Researchers [37], [30], [38] attempted using PU current signals for four operating conditions. Hoang et al. [37] achieved an average accuracy of 97.33% with a combined current signal using a DL method for three operating conditions. Lessmeier et al. [30] attempted an ensemble algorithm and attained 93.3% with phase current data for bearing fault classification. Karatzinis et al. [38] attained 91.42% accuracy for the fault classification with PU current signals using the fuzzy method.

The time–frequency domain-based machine learning fault diagnosis performance of current data is compared with other related works from PU bearing data shown in Table 13. However, the authors achieved an average accuracy of 99.8% with an FE-3 with *k*NN classifier under four operating conditions using current signals. The FE-3 consisting {MAV, SSI, WL} was found to be an optimal robust feature with good accuracy with simple time-domain features in comparison with other identified FEs using all the classifiers considered and also shows maximum accuracy of 100%.

Case study 2 investigates the KAIST PMSM's current dataset of stator interturn faults at different severities for the robustness of the identified FEs of case study 1. The results show 100% accuracy with the robust set of features FE-3 using *k*NN classifier.

In addition, the stability of the FEs is studied using experimental SCIM current data with a lower sampling rate and fewer data. The optimal robust FE-3 performs better for 3125 Hz, and 16 and 50 kHz sampling frequencies and shows an accuracy of 100% with the *k*NN under half and full load conditions. The optimal robust features perform better even at a low sampling rate.

Furthermore, the AlexNet neural network method using the SCIM current signals has an average accuracy of 98.7% with a computation time of 8040 s, which is 71% more computation time than the features-based fault diagnosis method. Since, it requires time–frequency image representation with a larger number of input images, as well as a GPU system. However, it needs to be noted that DL methods have been identified by their computational complexity, which necessitates the use of GPU hardware, as indicated in Table 14. Table 15 compares computational performance between the optimal robust features-based pattern recognition methods and a DL approach.

In addition, the adeptness of the identified optimal FEs is studied using run-to-failure NASA IMS bearing datasets using transient signals and shows a validation accuracy of 98.25% and 94.74% with the *k*NN and DT classifiers, respectively.

The optimal robust performance of mean absolute value, SSI, and WL have shown noticeable results among all the time-domain features analyzed. The identified optimal robust FEs have been successful in electrical machine fault identification with high accuracy and less computation burden in both steady state and transient conditions.

TABLE 14. Overview of Bearing Fault Diagnosis of Earlier Studies Contribution

Author	Year	Methodology	System specification
Jing-Xiao et al. [8]	2023	Attention-embedded quadratic network	NVIDIA RTX 3080Ti 12 GB GPU
Jiachen et al. [9]	2023	Joint adaptation network	GPU being NVIDIA GeForce RTX 2080 Ti
Sukanya et al. [32]	2023	Adaptive superlet transform and 2-D-CNN	NVIDIA GPU
Chun et al. [33]	2023	Multiscale residual attention and Multichannel network label-level	GTX 3060 GPU
Yifan et al. [34]	2023	Antinoise fault diagnosis network	NVIDIA RTX 3090Ti GPU with 24 GB RAM and four E-2224 CPUs
Hairui et al. [35]	2023	deep transfer clustering	NVIDIA RTX3070 GPU 8 GB GPU (NVIDIA
Yuhan et al. [36]	2023	Gramian angular field image and improved CNN	GeForce RTX 3060 6G)
Proposed method		Optimal robust features-based fault diagnosis	CPU Hardware

TABLE 15. Comparison of Computation Time

Method	Image/feature extraction method (s)	Classifier model (s)	Total computation time (min)
AlexNet method	840	7200	137
Optimal feature-based PR method	150	40	3.16

A. FUTURE SCOPE

Online monitoring provides a user interface that allows for the real-time monitoring and visualization of the current state of motor conditions. The purpose of an interface is to present sensor data patterns, diagnosis data, and alerts in a manner that is easy for operators and maintenance professionals to analyze. Employing a field-programmable gate array [39], [40] as a user interface for bearing diagnosis provides a robust and adaptable platform for building real-time monitoring systems with better performance.

VIII. CONCLUSION

Motor fault diagnosis using an optimal robust time-domain feature-based pattern recognition method is attempted to attain high accuracy with reduced computation time using motor current signals. Conventional and NCTDFs are attempted to identify the optimal feature ensembles using PSO from PMSM current signals under four distinct operating conditions. The optimal FE-3 was found to be good with all classifiers and attain maximum accuracy for combined current signals. Further, the optimal robustness of the identified FEs studied for PMSM stator interturn fault under eight distinct fault severities, and FE-3 was robust with all possible combinations. In addition, the stability of the identified FE was studied with experimental SCIM current signals with fewer samples in lower sampling frequencies at three different load conditions, and optimal FE-3 was found to be effective and attain high accuracy in comparison with the AlexNet method. In addition, the adeptness of the identified features was studied with run-to-failure bearing state and found to be effective in transient data classification. The identified optimal robust FE FE-3 consisting of {MAV, SSI, WL} maintains good classification accuracy with reduced computation time for bearing and stator fault diagnosis in PMSM and SCIM. A limitation of the optimal robust FEs is superior performance when applied to the combined phase current signal rather than to the individual phase current.

ACKNOWLEDGMENT

The authors would like to thank the Vellore Institute of Technology (VIT), Vellore, for providing the funds to support this research work in the Electrical Machines Laboratory, School of Electrical Engineering.

REFERENCES

[1] F. Huang et al., "Demagnetization fault diagnosis of permanent magnet synchronous motors using magnetic leakage signals," *IEEE Trans. Ind. Informat.*, vol. 19, no. 4, pp. 6105–6116, Apr. 2023.
[2] K. Yatsugi, S. E. Pandarakone, Y. Mizuno, and H. Nakamura, "Common diagnosis approach to three-class induction motor faults using stator current feature and support vector machine," *IEEE Access*, vol. 11, pp. 24945–24952, 2023.
[3] H. Pu, K. Zhang, and Y. An, "Restricted sparse networks for rolling bearing fault diagnosis," *IEEE Trans. Ind. Informat.*, vol. 19, no. 11, pp. 11139–11149, Nov. 2023.
[4] X. Chen, R. Yang, Y. Xue, M. Huang, R. Ferrero, and Z. Wang, "Deep transfer learning for bearing fault diagnosis: A systematic review since 2016," *IEEE Trans. Instrum. Meas.*, vol. 72, 2023, Art. no. 3508221.
[5] L. Frosini, "Novel diagnostic techniques for rotating electrical machinesâa review," *Energies*, vol. 13, no. 19, 2020, Art. no. 5066.
[6] M. Hakim, A. A. B. Omran, A. N. Ahmed, M. Al-Waily, and A. Abdellatif, "A systematic review of rolling bearing fault diagnoses based on deep learning and transfer learning: Taxonomy, overview, application, open challenges, weaknesses and recommendations," *Ain Shams Eng. J.*, vol. 14, no. 4, 2023, Art. no. 101945.
[7] R. Liu, B. Yang, E. Zio, and X. Chen, "Artificial intelligence for fault diagnosis of rotating machinery: A review," *Mech. Syst. Signal Process.*, vol. 108, pp. 33–47, 2018.

[8] J.-X. Liao, H.-C. Dong, Z.-Q. Sun, J. Sun, S. Zhang, and F.-L. Fan, "Attention-embedded quadratic network (qttention) for effective and interpretable bearing fault diagnosis," *IEEE Trans. Instrum. Meas.*, vol. 72, 2023, Art. no. 3511113.
[9] J. Kuang, G. Xu, T. Tao, Q. Wu, C. Han, and F. Wei, "Domain conditioned joint adaptation network for intelligent bearing fault diagnosis across different positions and machines," *IEEE Sensors J.*, vol. 23, no. 4, pp. 4000–4010, Feb. 2023.
[10] M. A. Jamil, M. A. A. Khan, and S. Khanam, "Feature-based performance of SVM and KNN classifiers for diagnosis of rolling element bearing faults," *Vibroengineering Procedia*, vol. 39, pp. 36–42, 2021.
[11] S. Sobhi, M. Reshadi, N. Zarft, A. Terheide, and S. Dick, "Condition monitoring and fault detection in small induction motors using machine learning algorithms," *Information*, vol. 14, no. 6, 2023, Art. no. 329.
[12] T. Li, C. Sun, O. Fink, Y. Yang, X. Chen, and R. Yan, "Filter-informed spectral graph wavelet networks for multiscale feature extraction and intelligent fault diagnosis," *IEEE Trans. Cybern.*, vol. 54, no. 1, pp. 506–518, Jan. 2024.
[13] C.-Y. Lee, T.-A. Le, and C.-L. Hung, "A feature selection approach based on memory space computation genetic algorithm applied in bearing fault diagnosis model," *IEEE Access*, vol. 11, pp. 51282–51295, 2023.
[14] M. Altaf, T. Akram, M. A. Khan, M. Iqbal, M. M. I. Ch, and C.-H. Hsu, "A new statistical features based approach for bearing fault diagnosis using vibration signals," *Sensors*, vol. 22, no. 5, 2022, Art. no. 2012.
[15] H. Tao, J. Qiu, Y. Chen, V. Stojanovic, and L. Cheng, "Unsupervised cross-domain rolling bearing fault diagnosis based on time-frequency information fusion," *J. Franklin Inst.*, vol. 360, no. 2, pp. 1454–1477, 2023.
[16] J. Tong, S. Tang, Y. Wu, H. Pan, and J. Zheng, "A fault diagnosis method of rolling bearing based on improved deep residual shrinkage networks," *Measurement*, vol. 206, 2023, Art. no. 112282.
[17] M. Alonso-González, V. G. Díaz, B. L. Pérez, B. C. P. G-Bustelo, and J. P. Anzola, "Bearing fault diagnosis with envelope analysis and machine learning approaches using CWRU dataset," *IEEE Access*, vol. 11, pp. 57796–57805, 2023.
[18] F. Yun, H. Dong, C. Liang, T. Weimin, and T. Chao, "Feature selection of XLPE cable condition diagnosis based on PSO-SVM," *Arabian J. Sci. Eng.*, vol. 48, no. 5, pp. 5953–5963, 2023.
[19] S. Alsudani and M. N. Saeea, "Enhancing thyroid disease diagnosis through emperor penguin optimization algorithm," *Wasit J. Pure Sci.*, vol. 2, no. 4, pp. 66–79, 2023.
[20] B. Wang, H. Li, X. Hu, and W. Wang, "Rolling bearing fault diagnosis based on multi-domain features and whale optimized support vector machine," *J. Vib. Control*, 2024, Art. no. 10775463241231344.
[21] N. Ganesh, R. Shankar, R. Čep, S. Chakraborty, and K. Kalita, "Efficient feature selection using weighted superposition attraction optimization algorithm," *Appl. Sci.*, vol. 13, no. 5, 2023, Art. no. 3223.
[22] H. Zhang, X. Chen, Z. Du, and R. Yan, "Kurtosis based weighted sparse model with convex optimization technique for bearing fault diagnosis," *Mech. Syst. Signal Process.*, vol. 80, pp. 349–376, 2016.
[23] T. A. Dhomad and A. Jaber, "Bearing fault diagnosis using motor current signature analysis and the artificial neural network," *Int. J. Adv. Scince Eng. Inf. Technol.*, vol. 10, no. 1, pp. 70–79, 2020.
[24] B. R. Nayana and P. Geethanjali, "Bearing fault detection: Feature selection algorithm efficacy study," *IETE J. Res.*, pp. 1–10, 2023.
[25] X. Zhong, T. Xia, and Q. Mei, "A parameter-adaptive VME method based on particle swarm optimization for bearing fault diagnosis," *Exp. Techn.*, vol. 47, no. 2, pp. 435–448, 2023.
[26] X. Ding, H. Wang, Z. Cao, X. Liu, Y. Liu, and Z. Huang, "An edge intelligent method for bearing fault diagnosis based on a parameter transplantation convolutional neural network," *Electron.*, vol. 12, no. 8, 2023, Art. no. 1816.
[27] W. Jung, S.-H. Yun, Y.-S. Lim, S. Cheong, and Y.-H. Park, "Vibration and current dataset of three-phase permanent magnet synchronous motors with stator faults," *Data Brief*, vol. 47, 2023, Art. no. 108952.
[28] A. H. Boudinar et al., "Induction motor bearing fault analysis using a root-music method," *IEEE Trans. Ind. Appl.*, vol. 52, no. 5, pp. 3851–3860, Sep./Oct. 2016.
[29] L. Cui, X. Tian, Q. Wei, and Y. Liu, "A self-attention based contrastive learning method for bearing fault diagnosis," *Expert Syst. with Appl.*, vol. 238, 2024, Art. no. 121645.
[30] C. Lessmeier, J. K. Kimotho, D. Zimmer, and W. Sextro, "Condition monitoring of bearing damage in electromechanical drive systems by using motor current signals of electric motors: A benchmark data set for data-driven classification," in *PHM Soc. Eur. Conf.*, vol. 3, no. 1, 2016.
[31] R. Nishat Toma and J.-M. Kim, "Bearing fault classification of induction motors using discrete wavelet transform and ensemble machine learning algorithms," *Appl. Sci.*, vol. 10, no. 15, 2020, Art. no. 5251.
[32] S. Mitra and C. Koley, "Early and intelligent bearing fault detection using adaptive superlets," *IEEE Sensors J.*, vol. 23, no. 7, pp. 7992–8000, Apr. 2023.
[33] C.-Y. Lee and G.-L. Zhuo, "Identifying bearing faults using multiscale residual attention and multichannel neural network," *IEEE Access*, vol. 11, pp. 26953–26963, 2023.
[34] Y. Jian et al., "LAFD-Net: Learning with noisy pseudo-labels for semisupervised bearing fault diagnosis," *IEEE Sensors J.*, vol. 23, no. 4, pp. 3911–3923, Feb. 2023.
[35] H. Fang, H. Liu, X. Wang, J. Deng, and J. An, "The method based on clustering for unknown failure diagnosis of rolling bearings," *IEEE Trans. Instrum. Meas.*, vol. 72, pp. 1–8, 2023.
[36] Y. Zhang, L. Shang, H. Gao, Y. He, X. Xu, and Y. Chen, "A new method for diagnosing motor bearing faults based on Gramian angular field image coding and improved CNN-ELM," *IEEE Access*, vol. 11, pp. 11337–11349, 2023.
[37] D. T. Hoang and H. J. Kang, "A motor current signal-based bearing fault diagnosis using deep learning and information fusion," *IEEE Trans. Instrum. Meas.*, vol. 69, no. 6, pp. 3325–3333, Jun. 2020.
[38] G. Karatzinis, Y. S. Boutalis, and Y. L. Karnavas, "Motor fault detection and diagnosis using fuzzy cognitive networks with functional weights," in *Proc. 26th Mediterranean Conf. Control Automat.*, 2018, pp. 709–714.
[39] J. Cureño-Osornio, I. Zamudio-Ramirez, L. Morales-Velazquez, A. Y. Jaen-Cuellar, R. A. Osornio-Rios, and J. A. Antonino-Daviu, "FPGA-flux proprietary system for online detection of outer race faults in bearings," *Electronics*, vol. 12, no. 8, 2023, Art. no. 1924.
[40] M. Kang, J. Kim, and J.-M. Kim, "An FPGA-based multicore system for real-time bearing fault diagnosis using ultrasampling rate AE signals," *IEEE Trans. Ind. Electron.*, vol. 62, no. 4, pp. 2319–2329, Apr. 2015.

G. GEETHA received the B.E. degree in electrical and electronics engineering from GTECH, Anna University, Chennai, India, in 2013, and the M.E. degree in power systems engineering from SRM Valliammai Engineering College, Anna University, in 2015. She is currently working toward the Ph.D. degree in fault diagnosis in electrical machines with the School of Electrical Engineering, Vellore Institute of Technology, Vellore, India.

Her research interests include condition monitoring of electrical machines, fault diagnosis, signal processing, image processing, machine learning, and deep learning.

Ms. Geetha was the recipient of the Anna University 18th rank holder for M.E. Power Systems Engineering from Anna University, Chennai, India, in 2015.

P. GEETHANJALI received the B.E. degree in electrical and electronics engineering from the University of Madras, Chennai, India in 2001, the M.Tech. degree in electrical drives and control from Pondicherry Engineering College, Puducherry, India, in 2004, and the Ph.D. degree in biomedical signal processing and control from the Vellore Institute of Technology, Vellore, India, in 2012.

Her research interests include biosignal and image processing, pattern recognition, the development of assistive devices, biomechanics, and the application of renewable energy in assistive devices.

Dr. Geethanjali was the recipient of the grants from the Department of Science and Technology (DST), Government of India. She was also the recipient of the Fulbright-Nehru Academic and Professional Excellence Fellowship for 2014–15. Her Ph.D. thesis has been nominated for âBest Thesisâ by the Indian National Academy of Engineering (INAE). She also recognized as top 2% of scientists list as per the survey conducted by Stanford University and Elsevier.